

Supplementary Information

for

**Comprehensive recycling of spent lithium-ion batteries  
cathodes and anodes *via* targeted electrochemical redox  
process†**

Shuai Gu,<sup>\*a</sup> Jiao Kong<sup>a</sup> and Baizeng Fang<sup>\*b</sup>

<sup>a</sup> *National Engineering Research Centre for Integrated Utilization of Salt Lake Resources, Joint International Laboratory for Potassium and Lithium Strategic Resources, School of Resources and Environmental Engineering, East China University of Science and Technology, Shanghai, 200237, China. Email: [gushuai@ecust.edu.cn](mailto:gushuai@ecust.edu.cn)*

<sup>b</sup> *School of Chemical Engineering and Energy Technology, Dongguan University of Technology, Dongguan 523808, Guangdong, China. Email: [baizengfang@163.com](mailto:baizengfang@163.com)*

**Table of Contents**

<b><u>1) Experimental details</u></b>	S3
<b><u>2) Analysis of the spent LIBs cathode material</u></b>	S4
Table S1 XRF, EDX, and ICP analyses of the spent cathode material	S5
Figure S1 SEM-EDX (a) and XRD (b) of the spent LIBs cathode	S5
<b><u>3) Crystal decomposition mechanism</u></b>	S6
<b><u>4) Leaching efficiency definition and leaching results</u></b>	S6
Figure S2 Leaching efficiency of Li <sup>+</sup> and Co <sup>2+</sup> in the form of cathode active powder and cathode sheet with 2 M HCl at 373 K	S7
Figure S3 Leaching efficiency of Li <sup>+</sup> (a) and Co <sup>2+</sup> (b) under different HCl concentrations	S7
Figure S4 Concentrations of Li <sup>+</sup> in the anode chamber with time at $E = 0.2V$	S8

Figure S5 Leaching efficiency of $\text{Al}^{3+}$ under different potentials	S8
Figure S6 Leaching efficiency of $\text{Li}^+$ and $\text{Co}^{2+}$ without copper foil at 343K	S9
Figure S7 Leaching efficiency of $\text{Li}^+$ (A) and $\text{Co}^{2+}$ (B) under different temperatures	S9
Table S2 Kinetics models used in the fitting process	S11
<b><u>5) Analysis and treatment of the leaching residue</u></b>	S12
Figure S8 SEM-EDX images of the cathode residue	S13
Figure S9 SEM-EDX images of the anode residue	S13
Figure S10 SEM (a) EDX (b) images of the treated cathode residue	S14
Figure S11 SEM-EDX images (a), size distributions (b), Raman image (c) and Raman shifts (d) of the treated anode residue	S14
<b><u>6) Energy consumption</u></b>	S14
<b><u>7) Pilot scale device and experiment</u></b>	S15
Figure S12 Eh-pH diagrams of Ni- $\text{H}_2\text{O}$ (a) and Mn- $\text{H}_2\text{O}$ (b) systems	S17
Figure S13 XPS survey of the cathode leached residue (a) and high-resolution XPS and the deconvoluted curves of Co 2p (b)	S17
<b>References</b>	S17

## **1) Experimental details**

Spent LIBs received from Alibaba Group Holding Ltd. were first discharged for 48 h in 0.5M NaCl solution to transport the majority of lithium from the anode to the cathode and avoid possible explosion/combustion during the disassembly process. Then, the discharged spent LIBs can be dismantled by hand or machinery, and to remove the electrolyte from the cathodes and anodes, rinsing with ethanol three times was adopted. After drying the cathodes and anodes at 60 °C for 2 h, the electrodes are ready to be recycled with the 2nd generation ECL. In industrial applications, the separation of the spent cathodes and anodes can be achieved by a photometric sorter. The photometric sorter uses ultraviolet, visible light, infrared rays, etc. to produce absorption, reflection, and transmission phenomena in contact with objects, detects materials, and then uses compressed air, water, or robotic arms to separate the anodes from the cathodes.

The potentials and voltages utilized in the manuscript are defined according to the general definitions, namely, the potential represents the half-cell potential vs. the reference electrode, while the voltages are the cell potential differences between the counter electrode and working electrode.

Electrochemical analysis and the targeted electroredox experiments were carried out in a traditional three-electrode system with KCl-saturated Ag/AgCl (0.197 V vs. SHE) as RE. The CV, Tafel, and CTTs analysis were carried out in a 10 mL electrolytic cell at 298 K with 5 mL of diluted HCl as the electrolyte, the spent LiCoO<sub>2</sub> plate (surface area: 2 mm × 5 mm) fixed by the electrode clip as the WE, a platinum plate (surface area: 20 mm × 20 mm) as the CE. The experiments were carried out in an H-type electrolytic cell (250 ml) in a traditional three-electrode system with the “sandwich-type” electrodes working as the WE (titanium mesh-cathode-titanium mesh) and CE (titanium mesh-anode-titanium mesh), respectively, and the KCl-saturated Ag/AgCl as the RE. The “sandwich-type” electrode consisted of a layer of titanium mesh (surface area: 50 mm × 50 mm), a layer of spent cathode (surface area: 40 mm × 40mm)/anode (surface area: 50 mm × 50 mm), and another layer of titanium mesh (surface area: 50 mm × 50 mm). The cathode and anode chambers were separated by

an anion exchange membrane (AEM) (AMI-7001). The current, potential, and  $E_{\text{cell}}$  were controlled and monitored by an electrochemical workstation (Gamry Reference 3000). XPS (Nexsa, Thermo Scientific), ICP-OES (Avio 200max, PerkinElmer) XRD (SmartLab, Rigaku), SEM-EDX (NanoSEM 450, FEI equipped with Falion 60S, EDAX, USA), particle size distribution (Mastersizer 3000, Malvern Panalytical) were utilized to obtain the compositions, structures, and morphologies of the solids. Surface pretreatment of the CE was performed by polishing the electrode surface with 1.0, 0.3, 0.05 micro gamma-alpha alumina powder in a sequence to a mirror finish and then being immersed in 3 mol/L HCl, acetone, methanol, and distilled water in an ultrasonic cleaner for 20 min, respectively, to remove any surface impurity. The electro-redox experiments were carried out in a 250 mL H-type electrolytic cell using 1M HCl as the electrolyte, an AEM was used to separate the cathode and anode chambers, 100 mL of electrolyte was added to the cathode and anode chambers, respectively. The electrolyte was deaerated by Ar prior to each experiment. All potentials, unless otherwise stated, are against the reference electrode (RE, saturated KCl Ag/AgCl electrode, 0.197 V vs. standard hydrogen electrode (SHE)).

## **2) Analysis of the spent LIBs cathode material**

The spent LIBs cathode material was first analyzed with XRF, SEM-EDX, and XRD. As can be seen from Table S1 and Fig. S1, the spent LIBs adopted in the experiments mainly consisted of  $\text{LiCoO}_2$  and  $\text{Li}_{0.98}\text{Co}_{1.04}\text{O}_2$ . The weight of metal in the 4×4 cm spent cathode and anode sheet was obtained by total dissolution of the spent sheet with 0.5 M HCl and 0.5 M VC at 363 K for 1 h and then analyzed with ICP-OES. And the weight of graphite in the spent anode is 147.1 mg.

**Table S1.** XRF, EDX, and ICP analyses of spent cathode material and anode materials

XRF	Co <sub>3</sub> O <sub>4</sub>	F	Al <sub>2</sub> O <sub>3</sub>	
wt%	95.34	3.59	1.07	
StdErr	0.21	0.42	0.05	
EDX	Co	F	Al	O
wt%	63.50	0.77	0.53	35.20
ICP-OES	Cathode sheet		Anode sheet	
Elements	Li <sup>+</sup>	Co <sup>2+</sup>	Al <sup>3+</sup>	Cu <sup>2+</sup>
mg	38.1	331.1	40.51	120.2

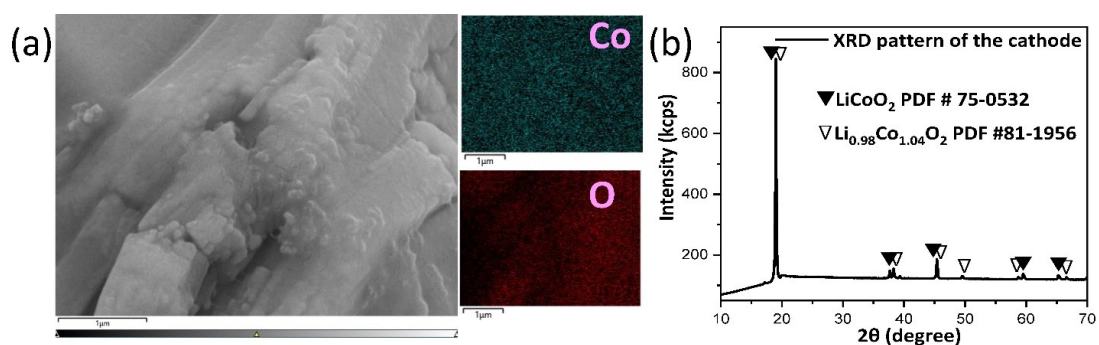


**Figure S1.** SEM-EDX (a) and XRD (b) of the spent LIBs cathode

### **3) Crystal decomposition mechanism**

By fitting the CTTs with the 2D instantaneous (Eqn. S1), 2D progressive (Eqn. S2), 3D instantaneous (Eqn. S3), and 3D progressive (Eqn. S4) equations, the crystal decomposition mechanism can be revealed.

$$i/i_m = t \exp\{-((t/t_m)^2 - 1)/2\}/t_m \quad (\text{S1})$$

$$i/i_m = (t/t_m)^2 \exp\{-2((t/t_m)^3 - 1)/3\} \quad (\text{S2})$$

$$(i/i_m)^2 = 1.9542[1 - \exp\{-1.2564(t/t_m)^2\}]/(t/t_m) \quad (\text{S3})$$

$$(i/i_m)^2 = 1.2254\{1 - \exp\{-2.3367(t/t_m)^2\}\}^2/(t/t_m) \quad (\text{S4})$$

where  $i$  represents the current density at time  $t$  after the potential step,  $i_m$  represents the maximum current density at time  $t_m$ .

### **4) Leaching efficiency definition and leaching results**

The leaching efficiency of metals was determined by Eqn. S5.

$$LE_{i(t,T)} = \frac{L_{i(t,T)}}{L_{i(T)} + F_i} \quad (\text{S5})$$

where  $LE_{i(t,T)}$  represents the leaching ratio of metal  $i$  at time  $t$  (time, unit: min) and temperature ( $T$ , unit: K);  $L_{i(t,T)}$  represents the concentration of metal  $i$  at  $t$  and  $T$ ;  $L_{i(T)}$  represents the final concentration of metal  $i$  in the leaching solution at corresponding  $T$ ;  $F_i$  represents the concentration of metal  $i$  in the residue.  $F_i$  was determined by dissolving the residue with the mixture of 0.5 M HCl and 0.5 M VC at 363 K for 1 h.

The leaching of  $\text{Li}^+$  and  $\text{Co}^{2+}$  in the form of cathode powder and cathode sheet with the same amount of cathode active materials was carried out. The results showed that the leaching ratios of both  $\text{Li}^+$  and  $\text{Co}^{2+}$  are low, and faster leaching kinetics of  $\text{Co}^{2+}$  was observed with the spent LIBs cathode sheets than with cathode powder (Figure S2b), indicating enhanced leaching of  $\text{Co}^{2+}$  with Al foil.

The leaching efficiency of  $\text{Li}^+$  and  $\text{Co}^{2+}$  increases with the increase of acid concentrations (Figure S3). Since lithium exists in both cathode and anode, lithium concentrations in the anode chamber were also monitored as shown in Figure S4, the lithium concentrations increased from 0 to 1.958 mg/L at 30 min. The dissolution of Al into the inorganic acids solutions is quite common (Figure S5). However, the leaching efficiency of Al is much higher in the present system. The mechanism for this phenomenon might be related to the nature of HCl. To decrease the dissolution rate of Al, a more diluted HCl or  $\text{H}_2\text{SO}_4$  solution can be utilized. Also, the effect of cell voltage on the dissolution ratio of Al can be studied in the future. Unlike  $\text{H}_2\text{SO}_4$  or  $\text{HNO}_3$ , HCl is a weak reducing acid and can destroy the oxidation layer formed on the surface of Al faster, thus, resulting in faster leaching efficiency and kinetics.

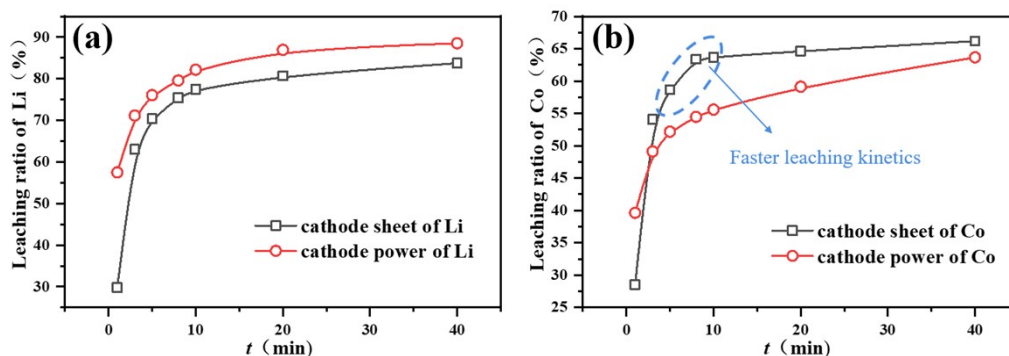


**Figure S2.** Leaching efficiency of  $\text{Li}^+$  (a) and  $\text{Co}^{2+}$  (b) in the form of cathode active powder and cathode sheet with 2M HCl at 373K.

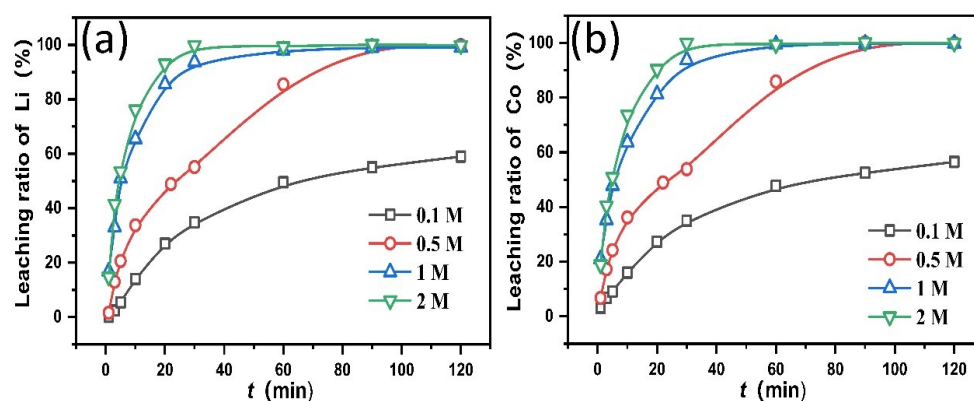


**Figure S3.** Leaching efficiency of  $\text{Li}^+$  (a) and  $\text{Co}^{2+}$  (b) under different HCl concentrations.

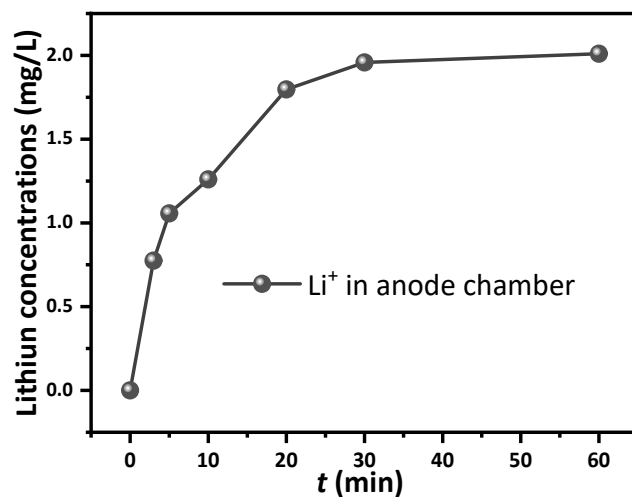


**Figure S4.** Concentrations of  $\text{Li}^+$  in the anode chamber with time at  $E = 0.2\text{V}$ .

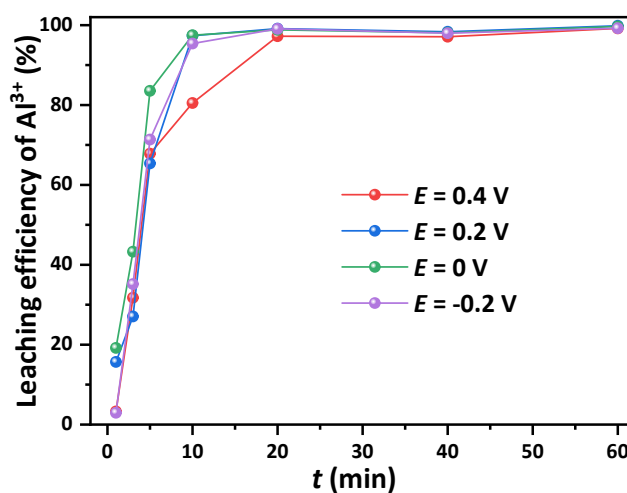


**Figure S5.** Leaching efficiency of  $\text{Al}^{3+}$  under different potentials.

Figure S6 shows the leaching efficiencies of  $\text{Li}^+$  and  $\text{Co}^{2+}$  without copper foil at 343 K. The results suggested that without the oxidization of Cu foil, the leaching efficiencies of  $\text{Li}^+$  and  $\text{Co}^{2+}$  were much smaller than that shown in Figure S7, indicating the vital role of Cu in the 2<sup>nd</sup> generation ECL.

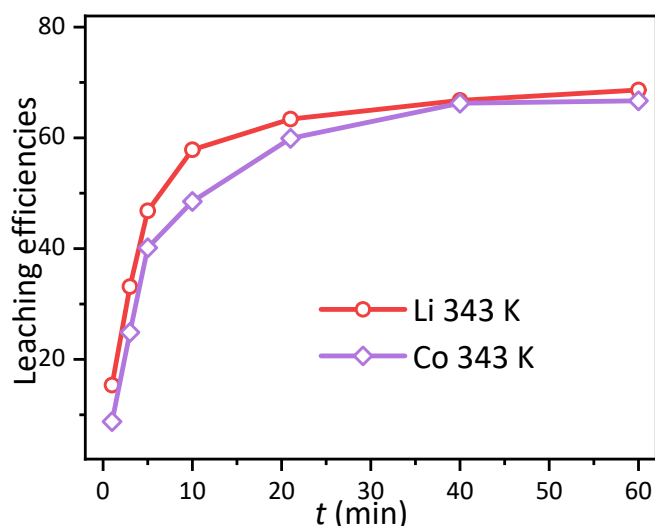


**Figure S6.** Leaching efficiency of  $\text{Li}^+$  and  $\text{Co}^{2+}$  without copper foil at 343 K.

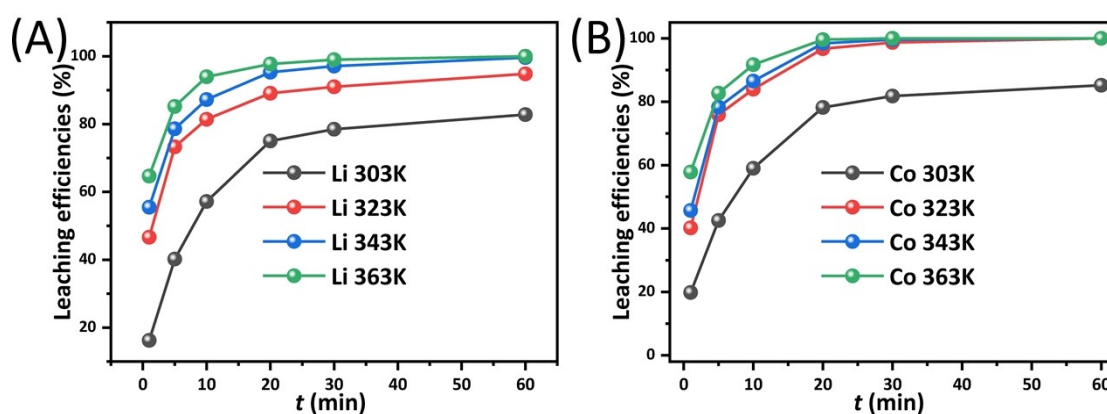


**Figure S7.** Leaching efficiency of  $\text{Li}^+$  (A) and  $\text{Co}^{2+}$  (B) under different temperatures.

The  $I-t$  curve of ECL at  $E = 0.2$  V shows a spontaneous chemical reaction at the first 10 min, which might be induced by the dissolution of Al in the cathode forming the galvanic cell, which generated the positive current. Because the positive current is not generated from the electrochemical workstation, the current efficiency of the ECL was calculated by dividing the amount of charge consumed reducing cobalt by the total amount of charge between 10 min and 60 min (eq S6). The amount of charge between 10 min and 60 min was calculated by integrating the current with time, while the amount of charge consumed reducing cobalt was calculated by multiplying the amount of cobalt reduced during 10 min and 60 min by Faraday's constant.

$$\eta = n * F * (C_{i60} - C_{i10}) * V * 100 / TC \quad (S6)$$

where  $\eta$  is current efficiency,  $n$  is the number of electrons transferred,  $F$  is the Faraday constant,  $C_{i60}$  is the concentration of species  $i$  at 60 min,  $C_{i10}$  is the concentration of species  $i$  at 10 min,  $V$  is the volume of the leaching solution,  $TC$  is the total amount of charges during 10 and 60 min.

The dissolution mechanism of spent LIBs cathode active material was analyzed with CTTs techniques. The leaching kinetics was fitted according to Table S2.

**Table S2.** A comprehensive summary of the kinetic models <sup>1,2</sup>

No.	Kinetic models	Name
<b>D1</b>	$kt = \alpha^2$	One-dimensional diffusion model
<b>D2</b>	$kt = (1-\alpha)\ln(1-\alpha)+\alpha$	Two-dimensional diffusion model
<b>D3</b>	$kt = [1-(1-\alpha)^{1/3}]^2$	Three-dimensional diffusion model (Jander)
<b>D4</b>	$kt = [1-(2\alpha/3)]-(1-\alpha)^{2/3}$	Ginstling-Brounshtein model
<b>D5</b>	$kt = [1/(1-\alpha)^{1/3}-1]^2$	Zhuravlev, Lesokhin and Templeman model
<b>D6</b>	$kt = [(1+\alpha)^{1/3}-1]^2$	Three-dimensional diffusion model (Anti-Jander)
<b>D7</b>	$k\ln t = [1-(1-\alpha)^{1/3}]^2$	Kroger and Ziegler model
<b>D8</b>	$kt = [1-(1-\alpha)^{1/2}]^2$	Cylindrical diffusion model (Jander)
<b>D9</b>	$kt = [1-(1+\alpha)^{1/2}]^2$	Cylindrical diffusion model (Anti-Jander)
<b>D10</b>	$kt = [1/((1-\alpha)^{1/3})]-1$	Dickinson and Heal model
<b>A1</b>	$kt = [-\ln(1-\alpha)]^{1/4}$	Avrami-Erofeev model
<b>A2</b>	$kt = [-\ln(1-\alpha)]^{1/2}$	Avrami-Erofeev model
<b>A3</b>	$kt = [-\ln(1-\alpha)]^{1/3}$	Avrami-Erofeev model
<b>A4</b>	$kt = [-\ln(1-\alpha)]^{4/3}$	Avrami-Erofeev model
<b>A5</b>	$kt = [-\ln(1-\alpha)]^{2/3}$	Avrami-Erofeev model
<b>A6</b>	$\ln k+n\ln t = \ln[-\ln(1-\alpha)]$	Avrami-Erofeev model
<b>F0</b>	$kt = \alpha$	Zero order
<b>F1</b>	$kt = -\ln(1-\alpha)$	First order
<b>F2</b>	$kt = (1-\alpha)^{-1}$	Second order
<b>R2</b>	$kt = 1-(1-\alpha)^{1/2}$	Interface (contracting area)
<b>R3</b>	$kt = 1-(1-\alpha)^{1/3}$	Interface (contracting volume)
<b>R4</b>	$kt = 1-(1-\alpha)^{2/3}$	Interface

<b>P1 (n=2)</b>	$kt = \alpha^{1/2}$	Power law (half)
<b>P1 (n=3)</b>	$kt = \alpha^{1/3}$	Power law (third)
<b>P1 (n=4)</b>	$kt = \alpha^{1/4}$	Power law (quarter)
<b>E1</b>	$kt = \ln\alpha$	Exponential
<b>E2</b>	$kt = [-\ln(1-\alpha)]^2$	Exponential
<b>B1</b>	$kt = \ln[\alpha/(1-\alpha)]$	Prout-Tompkins model

---

## **5) Analysis and treatment of the leaching residue**

The as-recovered residues from the cathode chamber (Figure S8) and anode chamber (Figure S9) were analyzed with SEM-EDX. SEM-EDX images of the cathode chamber suggested the total leaching of critical metals. The residue powder mainly consisted of the conductive agent and binder (PVDF). While the anode chamber powder mainly consisted of graphite and residual Cu. The conducting agent from the cathode residue was obtained by dissolving the PVDF in the residue with NMP and filtration (Figure S10). The treated cathode residue demonstrated small and even size distributions (around 100 nm). To test the reusability of the as-recovered anode residue, further processing was adopted. First, the as-recovered anode residue was washed with 1M HCl and 2wt% H<sub>2</sub>O<sub>2</sub> to remove any undissolved Cu, then the washed residue was washed again with NMP three times to remove the binder, finally, the residue was heated at 100 °C for 24 h and analyzed with SEM-EDX (Figure S11a) and laser particle sizer (Mastersizer 3000, Malvern Panalytical) (Figure S11b). And the voltage profiles of the recycled graphite were measured in a symmetric cell with 1.2 M LiPF<sub>6</sub> in ethylene carbonate working as the electrolyte, and lithium metals working as the counter electrode.

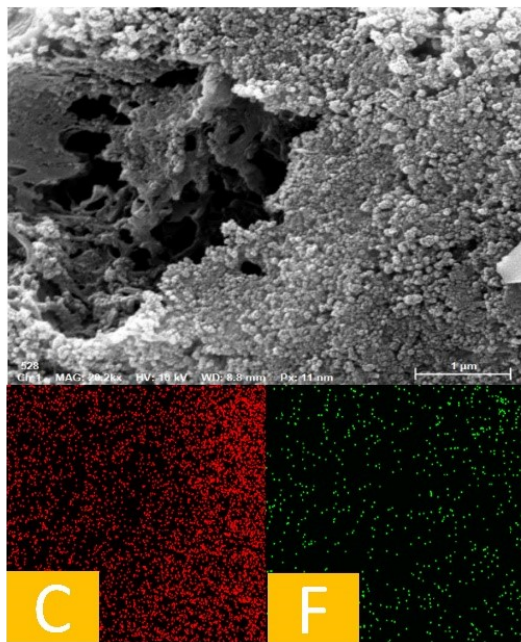


**Figure S8.** SEM-EDX images of the cathode residue.

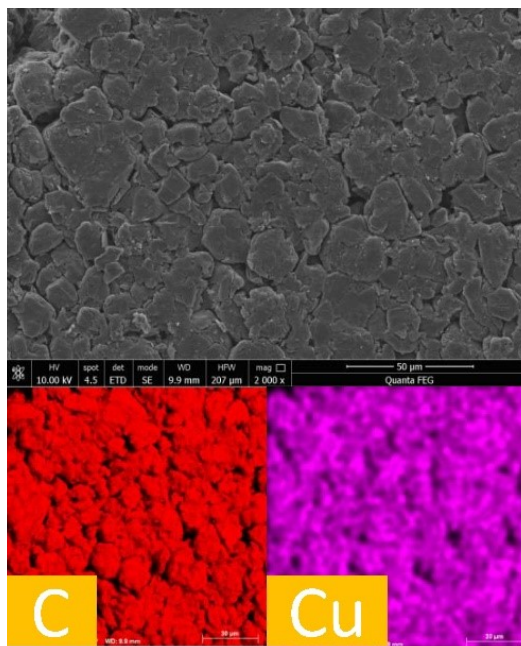


**Figure S9.** SEM-EDX images of the anode residue.

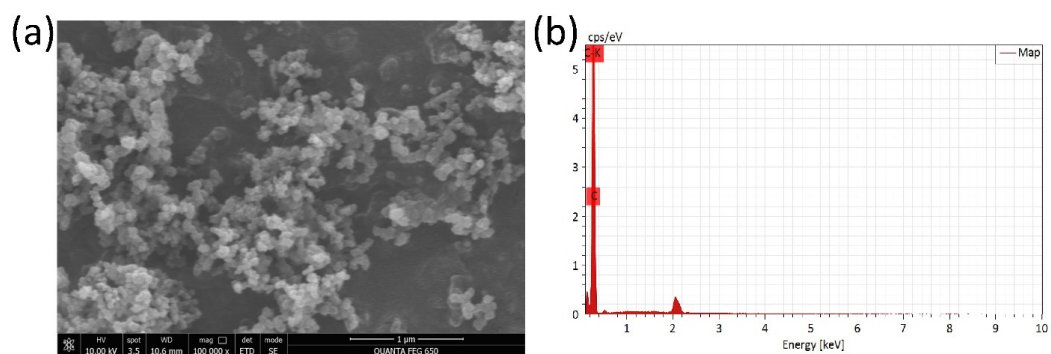


**Figure S10.** SEM (a) EDX (b) images of the treated cathode residue.

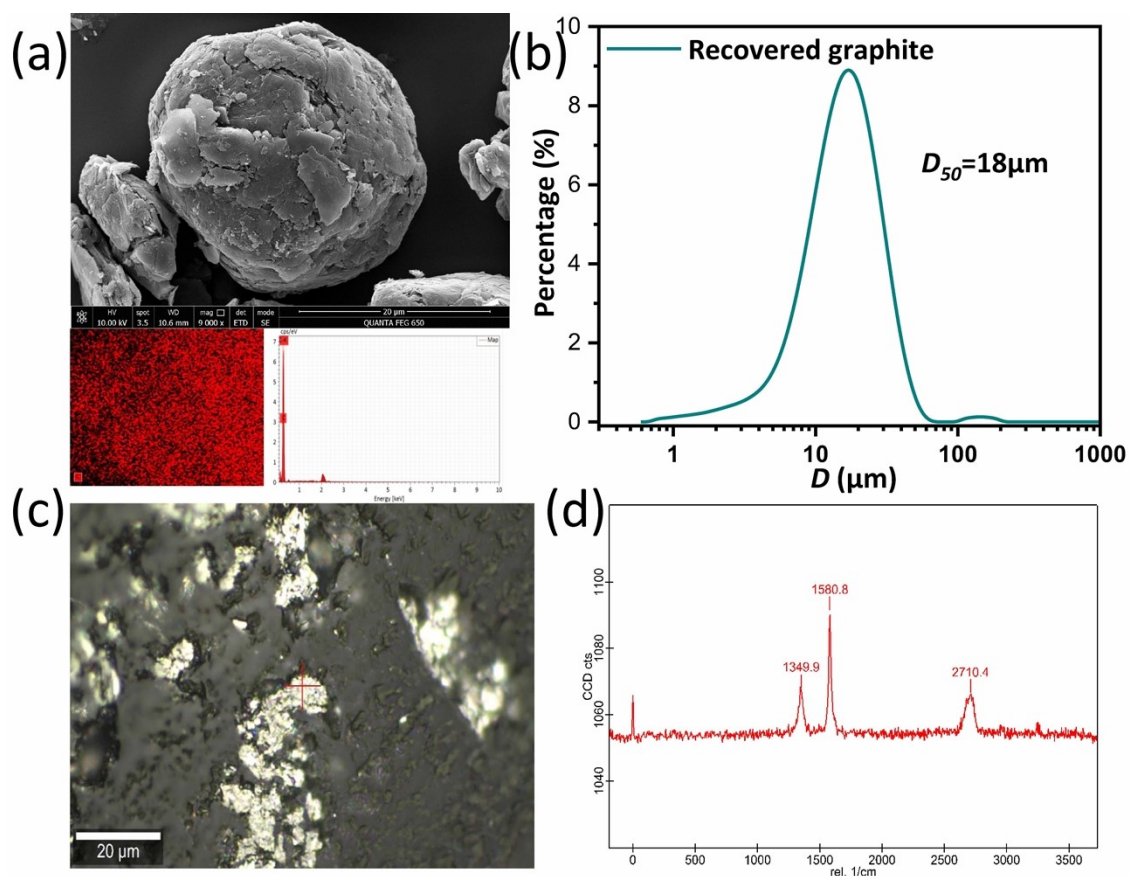


**Figure S11.** SEM-EDX images (a), size distributions (b), Raman image (c) and Raman shifts (d) of the treated anode residue.

From the SEM-EDX analysis, the recovered graphite is spherical with 100% carbon and has an average particle size of approximately 18  $\mu\text{m}$ . In addition, the results of the Raman

spectroscopy analysis shown in Figures S11 c and d indicate that the peaks at 1349.9, 1580.8 and 2710.4  $\text{cm}^{-1}$  correspond to the characteristic peaks of graphite.

## **6) Energy consumption**

The energy consumption estimations for producing cathode materials from primary and secondary resources. For primary sources, cobalt-containing minerals normally went through a relatively complicated process, e.g., copper-cobalt ore mining, ore milling and flotation, sulfating roast, leaching, solvent extraction, precipitation, evaporation and crystallization, and finally drying to obtain  $\text{CoSO}_4$ , while the most energy saving approach to extract lithium is from brine (only concentration and precipitation was needed). Due to the lack of energy conversion efficiency, only direct electricity consumption in both processes was considered, the energy consumption in other forms, i.e., diesel, natural gas, and steam, was omitted. For secondary resources, spent LIBs from cell phones were adopted. According to the 2<sup>nd</sup> generation ECL, the collected LIBs only went through the dismantling and ECL leaching process. After being obtained in the solution containing lithium and cobalt, the manufacturing process for both primary and secondary resources is the same, and thus, only the extraction process for lithium and cobalt was considered. The energy consumption data for producing lithium and cobalt from primary resources were calculated according to published LCA data<sup>3,4</sup> and Eqn. S7. While the energy consumption from 2<sup>nd</sup> generation ECL is calculated according to Eqn. S8.

$$W_P = W_{Li} + W_{Co} \quad (\text{S7})$$

$$W_S = W_1 + C * E_{cell}/M \quad (\text{S8})$$

where  $W_P$  and  $W_S$  are the energy consumption for producing 1M cobalt and 1M lithium from primary and secondary resources, respectively, unit: J/mol,  $W_{Li}$  and  $W_{Co}$  are the energy consumption for producing 1M lithium and 1M cobalt, respectively, unit: J/mol,  $W_1$  is the energy consumption from dismantling and stirring, unit: J/mol,  $C$  is the number of charges transferred during the 2<sup>nd</sup> generation ECL process, unit: C,  $E_{cell}$  is the cell voltage during the 2<sup>nd</sup>

generation ECL process, unit: V,  $M$  is the mole of lithium and cobalt leached into the cathode chamber, unit: mol.

## **7) Pilot scale device and experiment**

The pilot scale device consisted of a pair of metering pumps, liquid storage tanks (5 L), purge pipelines and liquid transfer pipelines, a plate and frame electrolyzer equipped with two pairs of “sandwich-type” electrodes and three membranes, and a DC supply. The leachate from the anode and cathode chamber was circulated by the metering pumps at the same liquid flux (115 L/h) for 2 h and according to the cell voltage ( $E_{cell}$ ) obtained from Fig. 4 from the traditional three-electrode system,  $E_{cell} = 0.4$  V was adopted for the pilot scale experiment. The surface area of the titanium mesh electrode for the “sandwich-type” electrode was 485.76 cm<sup>2</sup> (26.4 cm × 18.4 cm) and a membrane was used to separate the cathode chamber from the anode chamber. 700 g of the cathode (including active material and Al foil) and 568 g of the anode (including active material and copper foil) were obtained from mixed spent LIBs and arranged evenly between the “sandwich-type” cathode and anode electrode, respectively. More electrodes can be installed in the plate and frame electrolyzer if more spent cathodes and anodes are available. The pilot scale plate and frame electrolyzer were clamped together with bolts and kept tight during the whole leaching process. Eh-pH diagrams of Ni-H<sub>2</sub>O and Mn-H<sub>2</sub>O systems indicated that the ECL behavior of Ni and Mn is similar to that of Co and cathode active materials containing Ni, Co, and Mn can all be leached during the ECL (Figure S12). The whole pipeline was purged three times and all liquid/residue was collected and analyzed with ICP-OES to determine the leaching efficiency and recovery yield. The residue from the anode chamber was washed with 1M HCl and 2wt% H<sub>2</sub>O<sub>2</sub> to remove any undissolved Cu, then the washed residue was washed with NMP three times to remove the binder, finally, the residue was heated at 100 °C for 24 h and weighted with an electronic balance to obtain the yield of graphite. The leaching residue in the cathode chamber after 2h was analyzed with XPS (Figure S13a), and the residual Co in the residue mainly existed in the form of Co<sub>3</sub>O<sub>4</sub> and CoO (Figure S13b). The amount of H<sub>2</sub> gas generated during the ECL process was measured by collecting all the gas in the pilot device and pipeline with Ar carrier gas. And around 10 L of gases including

Ar gas were collected and the total volume of H<sub>2</sub> generated was 0.29 L (measured with gas chromatography/mass spectrometer GC-MS, HP-5, Agilent 8890-5977B). As for the 1st ECL, based on the data reported by Prabakaran, G. et al. (Prabakaran, G.; Barik, S. P.; Kumar, N.; Kumar, L. Electrochemical process for electrode material of spent lithium-ion batteries. Waste Manag. 2017, 68, 527–533.), the amount of H<sub>2</sub> generated for processing 150 g sample were 1.1 L and if the same amount of materials (729 g) were to processed with the above method 5.35 L H<sub>2</sub> would be generated. Thus, the proposed 2nd ECL can successfully suppress the HER during the ECL.

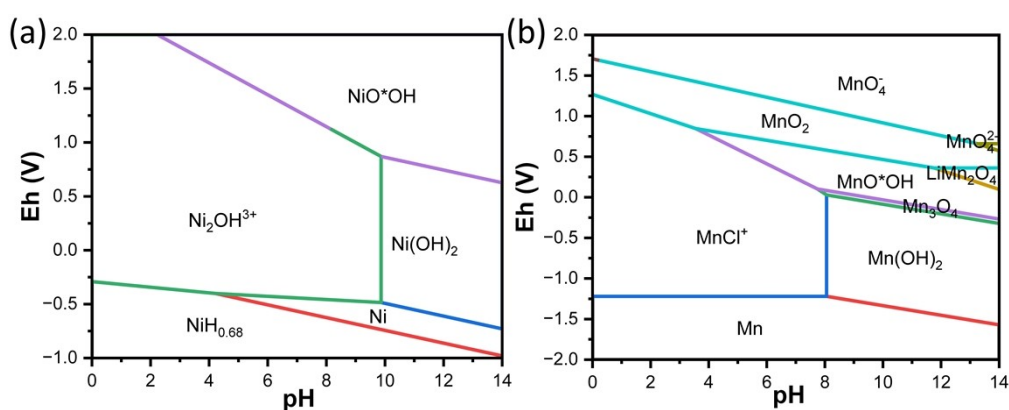


**Figure S12.** Eh-pH diagrams of Ni-H<sub>2</sub>O (a) and Mn-H<sub>2</sub>O (b) systems.

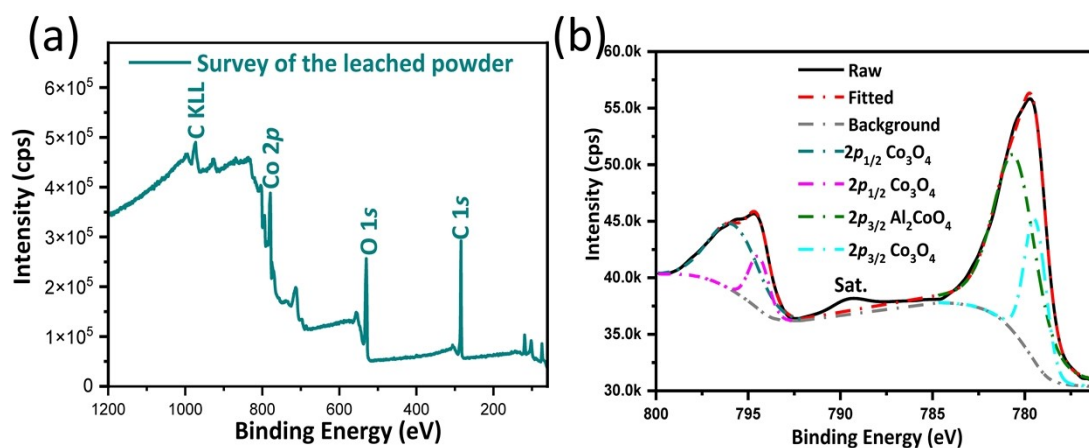


**Figure S13.** XPS survey of the cathode leached residue (a) and high-resolution XPS and the deconvoluted curves of Co 2p (b).

## References

- [1] C.F. Dickinson, G.R. Heal, *Thermochimica Acta* **1999**, 340-341, 89-103.
- [2] J. H. Sharp, G. W. Brindley, B. N. N. Achar, *J. Am. Ceram. Soc.* **1966**, 49, 379-382.
- [3] Q. Dai, J. Kelly, A. Elgowainy, Cobalt Life Cycle Analysis Update for the GREET® Model, Argonne National Laboratory, **2018**.
- [4] J. C. Kelly, M. Wang, Q. Dai, O Winjobi, *Resour. Conserv. Recycl.* **2021**, 174, 105762.